JOURNAL OF AIRCRAFT
Vol. 42, No. 3, May–June 2005

Transonic Experimental Observations of Abrupt Wing Stall on an F/A-18E Model

S. Naomi McMillin,* Robert M. Hall,† and John E. Lamar†
NASA Langley Research Center, Hampton, Virginia 23681

A transonic wind-tunnel test of an 8% F/A-18E model was conducted in the NASA Langley Research Center 16 ft Transonic Tunnel to investigate on-surface flow physics during stall. The technical approach employed focused on correlating static (or time-averaged) and unsteady wind-tunnel test data to the unsteady wing-stall events using force, moment, pressure, and pressure-sensitive-paint measurements. This paper focuses on data obtained on the preproduction configuration of the F/A-18E aircraft at Mach number of 0.90. The flow unsteadiness occurring on the wing as the wing went through the stall process was captured using the time histories of balance and pressure measurements and by calculating the root mean square (rms) for a number of instrument signals. The second step was to gather global perspectives on the pressures influencing the wing-stall process. The abrupt wing stall experienced by the 8% F/A-18E model was observed to be an unsteady event triggered by the rapid advancement of separation, which had migrated forward from the trailing edge, to the leading-edge flap hingeline over a very small increment in angle of attack. The angle of attack at which this stall occurred varied, from run to run, over a 1-deg increment. The abrupt wing stall was observed, using pressure-sensitive paint, to occur simultaneously on both wing panels or asymmetrically. The pressure-sensitive-paint data and wing-root bending-moment data were essential in providing insight to the flow structures occurring over the wing and the possible asymmetry of those flow structures. A repeatability analysis conducted on eight runs of static data provided a quick and inexpensive examination of the unsteady aerodynamic characteristics of abrupt wing stall. The results of the repeatability analysis agreed extremely well with data obtained using unsteady measurement techniques. This approach could be used to identify test conditions for more complex unsteady data measurements using special instrumentation.

Nomenclature

BL	=	semispan station measured from aircraft centerline, full-scale length, in.
C_A	=	axial-force coefficient
C_D	=	drag-force coefficient
C_L	=	lift-force coefficient
C_l	=	rolling-moment coefficient
C_m	=	pitching-moment coefficient
C_N	=	normal-force coefficient
C_n	=	yawing-moment coefficient
C_p	=	wing surface-pressure coefficient
C_{WM}	=	wing-root bending-moment coefficient
C_y	=	side-force coefficient
c	=	local wing chord
M	=	freestream Mach number
x	=	distance on wing planform from the wing leading edge, in.
α	=	angle of attack, deg
α_{st}	=	angle of attack where the C_L vs α curve had a significant break in slope
β	=	sideslip angle, deg
σ	=	standard deviation

Introduction

THE Abrupt Wing Stall (AWS) program has been an applied aerodynamics effort addressing uncommanded lateral motions, a challenge that has plagued a significant number of aircraft over at least the last 50 years. The impetus of this program was the wing drop encountered during the engineering, manufacturing, and development phase of the F/A-18E/F program (see Ref. 1). Figure 1 shows a picture of the F/A-18E/F aircraft. After significant expenditure of flight test and analysis resources, the lateral activity was mitigated by flight-derived fixes for the F/A-18E/F, and the aircraft proceeded into production phase. However, the fact remains that the lateral instability was not predicted prior to flight testing. Consequently, a cooperative NASA/Navy/Air Force program was charged with developing methods and procedures to analyze and predict uncommanded motions for future aircraft.

A key component of this research was a series of wind-tunnel test programs to investigate the abrupt-wing-stall phenomenon and develop a strategy for future testing and analysis of aircraft susceptible to abrupt wing stall. The program had the advantage of access to several databases from the F/A-18E/F developmental program including transonic wind-tunnel force and moment data and oil flow visualization, Navier–Stokes computations, and flight-test data. Based on a study of these databases, an experimental strategy was developed to fill in the flow understanding "gaps" surrounding the abrupt-wing-stall phenomena as exhibited by an F/A-18E model (preproduction configuration). The technical approach employed focused on correlating static (or time-averaged) and unsteady wind-tunnel test data to the unsteady wing-stall events using force, moment, pressure, and pressure-sensitive-paint measurements.

The paper describes the wind-tunnel model, instrumentation, data-acquisition techniques, analysis results, and the interpretation of the data as it relates to an improved understanding of the abrupt-wing-stall phenomenon as it occurred on the preproduction baseline configuration using the 8% F/A-18E model. To obtain approval for releasing this paper to the public, quantitative information has been removed from most vertical scales as per guidelines from the U.S. Department of Defense.

Technical Approach

A two-step approach was used in the correlation of static wind-tunnel data and unsteady wing stall occurring on an 8% model of the preproduction F/A-18E/F aircraft. The first step in this technical

Presented as Paper 2003-0591 at the AIAA 41st Aerospace Sciences Meeting, Reno, NV, 6–9 January 2003; received 16 June 2003; revision received 6 January 2004; accepted for publication 9 January 2004.

*Aerospace Engineer, M/S 499, Configuration Aerodynamics Branch.
†Aerospace Engineer, M/S 499, Configuration Aerodynamics Branch. Associate Fellow AIAA.

Fig. 1 Photograph of the F/A-18E/F aircraft.

approach was to capture the unsteadiness occurring on the wing as the wing went through the stall process. The second step was to gather global perspectives on the pressures influencing the wing-stall process. In carrying out these steps, several experimental techniques were employed in two test entries in the Langley 16-ft Transonic Tunnel (16-ft TT).

Model and Instrumentation Description

The 8% F/A/-18E model was modified to accommodate six sets of instruments. The instrumentation included the following types: static, unsteady, and optical.

Model Description

The model tested in the Langley 16-ft TT was an 8% model of the F/A-18E aircraft. The model has a span of 43.1 in. and a length of 55.0 in. The model geometry was the same as the preproduction F/A-18E configuration. In fact, this particular model was the test article in the F/A-18E/F program for the development of this aircraft and had been used previously for tests in the Veridian 8-ft transonic tunnel. The model was originally designed to hold a six-component internal balance and steady pressure ports on the fuselage and ducts. The model was modular in nature, such that the wings, ducts, and tails could be removed and replaced with different geometries. This modularity allowed two new wing spars and flaps to be fabricated and used on the existing fuselage. The new wings had the identical geometry as the preproduction wing geometry of the F/A-18E. The wing did not include the porous wing fold fairing arrangement of the production aircraft. Rather, the fold fairing door was solid for the current investigation.

Transition trip dots were placed on the model in order to trip the boundary layer during wind-tunnel testing. Each cylindrical dot had a diameter of 0.05 in. and a height of 0.004 in. The dots were installed with an edge-to-edge spacing of 0.025 in. The trip dots were located 0.40 in. aft (measured in a streamwise direction) from the tip of the fuselage nose and 0.40 in. aft (streamwise, on both sides) from the leading edges of the wings, leading-edge extension (LEX), horizontal and vertical tails. The trip dots were also located on the external surfaces of each inlet cowl, similarly at 0.40 in. aft (streamwise) from the leading edges.

This paper deals solely with the preproduction baseline geometry tested in the F/A-18E/F development program with a 10 deg/10 deg/5 deg flap set where the deflection notation corresponds to the leading-edge flap deflection, the trailing-edge flap deflection, and the aileron deflection, respectively. This configuration is referred to hereafter as the baseline configuration. This flap set is representative of the 6.1.3 version of the flight control laws developed as the "80% solution" to the abrupt-wing-stall problem as it occurred in the aircraft development program.

Instrumentation Description

Six sets of instrumentation were used in the test program: 1) an internal six-component strain-gauge balance, 2) three internal 64-port electronic scanning pressure (ESP) modules for sampling 168 wing steady pressure ports, 3) 22 unsteady wing pressure transducers, 4) four outer-wing accelerometers, 5) two wing-root bending-moment strain gauges, and 6) a pressure-sensitive-paint flow visualization system.

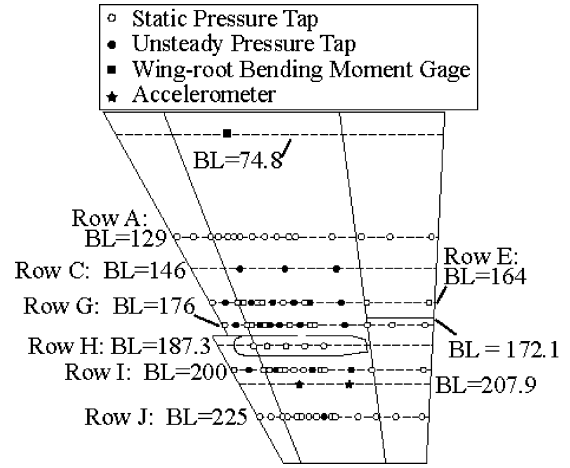

Fig. 2 Sketch of instrumentation layout on the upper surface of left heavily instrumented wing. Units are in inches and are full-scale measurements.

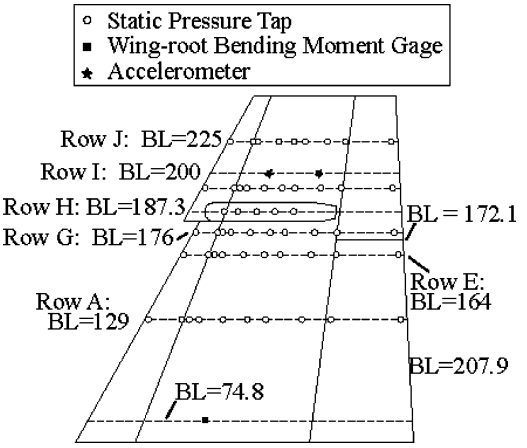

Fig. 3 Sketch of instrumentation layout on the upper surface of the right instrumented wing (same layout for left lightly instrumented wing). Units are in inches and are full scale measurements.

Three wing panels were fabricated. Two versions of the wing panel were used. The first left wing panel, referred to as the heavily instrumented wing panel, was instrumented to obtain unsteady data simultaneously with static data on the surface of the wing. This panel contained steady pressure ports, in situ unsteady pressure transducers, outer-wing accelerometers, and wing-root bending-moment gauges. The majority of pressure ports were located on the upper surface of the wing as shown in Fig. 2. The lower surface, not shown here, had a much smaller number of orifices. Lower surface data are not presented here.

Because of instrumentation complexity and cost, the right wing panel had no unsteady wing pressure transducers and a reduced number of steady pressure ports as shown in Fig. 3. The third wing panel, a left wing panel that mirrored the reduced instrumentation of the right wing, was fabricated for obtaining pressure-sensitive-paint data simultaneously with static data. Thus, unsteady pressure ports were not included on this left wing panel or the right wing panel because the instrumentation would not survive the harsh chemicals used to apply and remove the coats of pressure-sensitive paint.

Experimental Approach

The first step in the technical approach was to capture the unsteadiness occurring on the wing as it went through the stall process. This step was accomplished using three data-acquisition techniques: repeat runs, rms signals, and time histories. The second step was to gather global looks at the pressures influencing the wing-stall

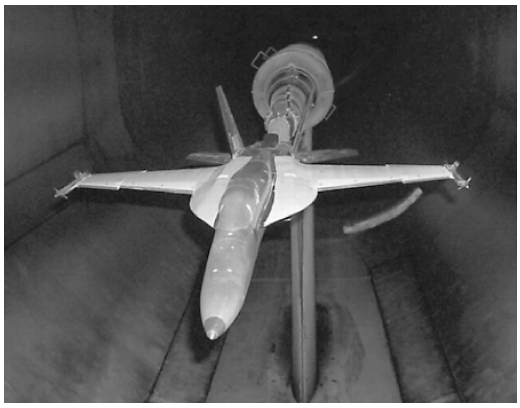

Fig. 4 Photograph of the 8% F-18E model in the 16-ft TT.

process. This step was accomplished using the pressure-sensitive-paint (PSP) technique, with its advantage of providing continuous pressure information across the span, rather than at the discrete spanwise locations associated with pressure ports.

Data were obtained using the pitch-pause method during runs of the model. The model was initially set at a low angle of attack, typically $\alpha = -4$ deg. Then the model was pitched to the next desired angle of attack and, then, paused for 20–60 s depending on the type of measurements being taken. The model was pitched in 0.5-deg increments upto $\alpha = 15$ deg.

Tunnel and Flow Conditions

The model was tested in the 16-ft TT at NASA Langley Research Center. The 16-ft TT is a single-return, continuous-flow, atmospheric tunnel with air exchange and a slotted octagonal test section. A complete description of this wind tunnel and its operating characteristics is presented in Ref. 2. Figure 4 shows the model installed in tunnel test section. Note that a coat of pressure-sensitive paint has been applied to the upper surface of the wing.

Testing was performed at atmospheric conditions for $0.5 \leq M \leq 0.9$. Data were obtained over the angle of attack α range of -4 to 16 deg and over the sideslip angle β range of -5 to 5 deg. The intention of this paper is to limit the data review to those factors that define the flow phenomena associated with the abrupt-wing-stall issue. Thus, this paper discusses only data obtained over the α range on the preproduction baseline F/A-18E geometry with a 10 deg/10 deg/5 deg flap setting at $M = 0.9$ and $\beta = 0$ deg.

The data examined in this study were obtained in a pitch-pause mode. At the beginning of an α sweep, the model would initially be set to $\alpha = -4$ deg. The model would then be pitched up in increments of 0.5 deg with a 10–20 s pause between increments. Instrumentation measurements and PSP photographs were taken during this pause. When the model was tested at wing-stall conditions, the model visibly exhibited significant dynamic motions, which were combinations of pitch, plunge, and roll. The intensity of the dynamic motions varied from run to run for the same configuration. Repeat runs would often have different intensity levels in dynamic motions. The testing procedure included monitoring the balance for proximity to the balance force and moment limits. During the α range associated with abrupt wing stall, it was not uncommon for the balance limits to be exceeded. When this occurred, the model angle of attack was quickly increased and the motions subsided, or Mach number was quickly decreased. The model exhibited this vibration whether the model approached the critical α range from lower or higher angles of attack.

Static Data

To further understand and correlate with the unsteadiness of the stall process, time-averaged data were obtained to understand the flow structure over the wing before the stall occurred. The static data obtained were configuration force/moment data, wing surface-pressure data, and wing-root bending-moment data. The static data were obtained using the data-acquisition system of the 16-ft TT. The signals from the various equipment were passed through a low-pass filter (1 Hz) and then sampled for 5 s at a 10 sample/s rate. The average of the samples was then used as static data (also referred to as time-averaged data).

Repeat Runs

Because previous testing showed that the model would vibrate on the sting/strut assembly in the tunnel at wing-drop conditions, it was necessary to determine the repeatability of the static data in this α range. A series of repeat runs was therefore conducted in each test entry. The repeat runs were conducted on the baseline configuration at $M = 0.9$. The baseline configuration was installed at the beginning, middle, and end of a test entry. Several back-to-back runs were obtained for each baseline configuration installation. A simple statistical analysis was conducted on the set of repeat runs for each test entry. As discussed in a later section, data from the repeatability analysis were found to correspond extremely well with other markers of the flow unsteadiness.

RMS Measurements

Another effort made to capture the character of the flow unsteadiness involved routing the signals from the balance, unsteady pressure transducers, wing strain gauges, and outer-wing accelerometers through rms boards that calculated running values of rms for the respective signals. This value of the rms was then recorded by the usual time-filtered tunnel data-acquisition system. These rms signals do not, of course, contain any information as to the frequency or character of the true time history.

Time History Measurements

The second, more resource intensive, level of unsteadiness measurement was to record the time histories of various parameters. The dynamic data-acquisition system employed in this effort was capable of acquiring time-synchronized data on 32 channels. Three balance channels, 23 unsteady pressure transducers, two wing-root bending-moment gauges, and the four outer-wing accelerometers were dynamically sampled. The three balance channels chosen for dynamic sampling were the axial-force, pitching-moment, and rolling-moment components.

During the test, the unsteady data were acquired in 10-s records on magnetic tape using VHS videocassettes and digitized posttest. In the digitizing process, the data were sampled at a rate of 1000 samples per second for 10 s. A 200-Hz antialiasing filter was applied to data during the digitization process. Time history records, mean, standard deviation, and maximum and minimum values were processed for each data point and channel in the data set. The data were stored on a compact disk volume for further data processing by the AWS team. Initial data analysis from this data set is discussed in Ref. 3.

Pressure-Sensitive-Paint Measurements

The second entry of the model focused on gathering global looks at the pressures influencing the wing-stall process through the use of the PSP technique. Figure 4 shows a photograph of the model with a coating of PSP on the upper surface of the wings as installed in the 16-ft TT. Reference 4 contains a more detailed description of the PSP testing technique. The discussion here will cover some details that significantly influenced the testing.

Before a PSP coating could be applied, the surface of the model had to be at room temperature. This limitation required extensive down time between configuration changes because the model would heat up significantly during a test run. Once the PSP coat was applied and dry, the registration marks could be applied and measured. Overall, the time consumed in the application process is a limiting factor in the use of this technique in the wind-tunnel testing environment.

Another time-consuming task in the PSP process was the necessity to take wind-off images after each wind-on run. This step look longer than the actual wind-on run because the wind-off images were acquired at finer angle-of-attack increments than those taken

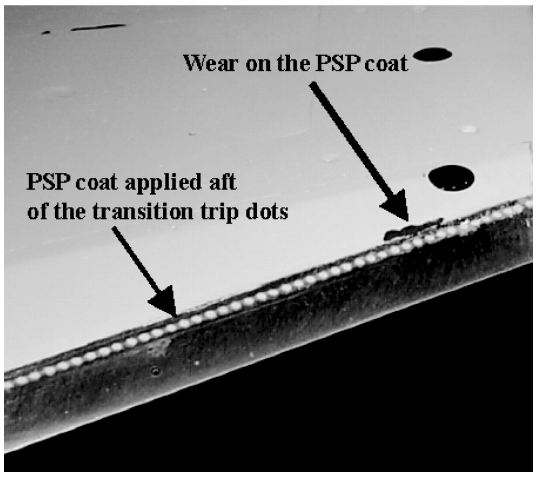

Fig. 5 Photograph of wing leading edge with trip dots and PSP coat.

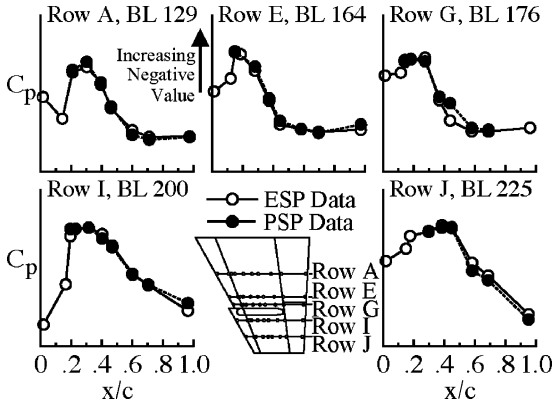

Fig. 6 Comparison of measured ESP and calculated PSP data at $\alpha = 8$ deg (run 1334).

in the actual wind-on run. This step was necessary to find a suitable wind-off image corresponding to each wind-on image in the calibration process.

Figure 3 shows the locations of the measured pressure ports used to calibrate the PSP images. The PSP coat was applied to the surface of the wing aft of the trip dots, as shown in Fig. 5. Therefore, the first pressure port in each row was not used in the calibration. Other ports were eliminated on a case-by-case basis as a result of bad pressure port data, extreme pressure gradients occurring directly over the port, or inability of the calibration algorithm to accommodate a specific data point.

Recall that a static measurement is an average of 50 samples of data acquired over a 5-s time period. In contrast, the PSP photographic image is acquired over a much shorter time period of 1.5 s. The acquisition of both the ESP and PSP data began at the same time. To check the calibration of the PSP data, the measured pressures from the static pressure data (referred to hereafter as ESP data) were compared with pressures resulting from the PSP data reduction algorithm at the ports used for the calibration. Figure 6 shows a sample comparison for $\alpha = 8.0$ deg on the left wing panel. All data presented in this paper will be for $M = 0.90$. The comparison of ESP measured and PSP calibrated data is remarkably good. This result is also present on the right wing and even in the α range of abrupt stall (data not shown here).

The upper surface of the wing was fabricated with trenches, which contained the pressure tubing and wiring. The trenches were filled in with body fill material. Because this fill material has different thermal characteristics than the steel of the model, the PSP results were affected slightly over these areas. Although the PSP postprocessing was able to eliminate much of this effect, some shadows of the trenches remain in the PSP images, as seen in Fig. 7.

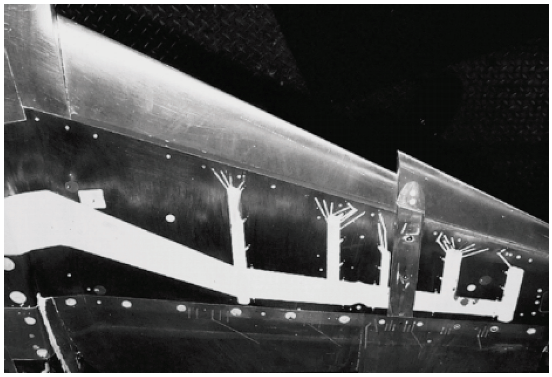

a) Bare model—trenches in white paint

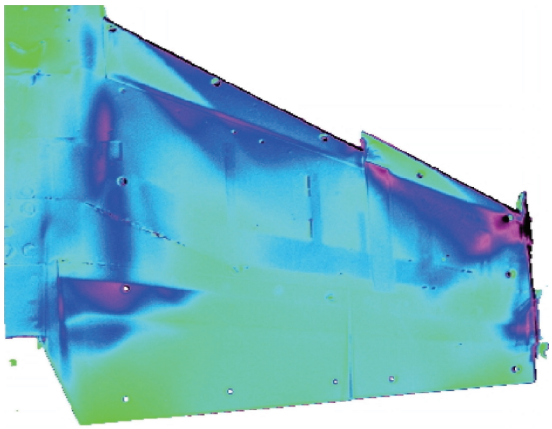

b) PSP image at $\alpha = 10.0$ deg (run 1334)

Fig. 7 Effect of trench fill material on the PSP image.

Figure 8 compares a PSP image with an oil flow obtained in a previous entry of this model with the original uninstrumented wings in the Veridian tunnel. Both sets of data are for the baseline configuration at $M = 0.9$ and $\alpha = 8.0$ deg. The flow features are captured by both techniques as identified in the figure. The PSP technique can capture more angles of attack in a given run than the oil flow technique.

The postprocessing of the PSP images is time intensive and not automatic. One feature of the process is assigning color to pressure values. A color bar, which assigns a maximum and minimum value to the extremes of the color bar, is generated. For the sake of comparison in this paper, all of the PSP images used the same color bar, even though the maximum and minimum values of each image were different.

Analysis of Abrupt Wing Stall

Over 500 data runs were obtained from the two test entries of the 8% F/A-18E model in the 16-ft TT. These data define the effects of test conditions and variations of the model in detail. Discussion of the full data set is beyond the intended scope of this paper. The baseline configuration is defined as the configuration with the baseline flap geometry with flaps set at 10 deg/10 deg/5 deg. The following discussion is limited to the baseline configuration at $M = 0.9$, $\beta = 0$ deg, and over an angle-of-attack range of -2 to 14 deg.

Static Data and Pressure-Sensitive-Paint Data

Figure 9 shows the lift, rolling moment, and wing-root bending-moment coefficient data (C_L, C_l, and C_{WM}, respectively) for the baseline configuration at $M = 0.9$ over an angle-of-attack range of -2 to 14 deg. The angle of attack at which wing stall occurs, α_{st}, is defined as the angle of attack where the C_L vs α curve has a significant break in slope. The C_L data of Fig. 9 show that for run 1334 $\alpha_{st} = 9.1$ deg. The left and right C_{WM} data indicate that the wing stall is not symmetrical. The right-wing panel stalls before the

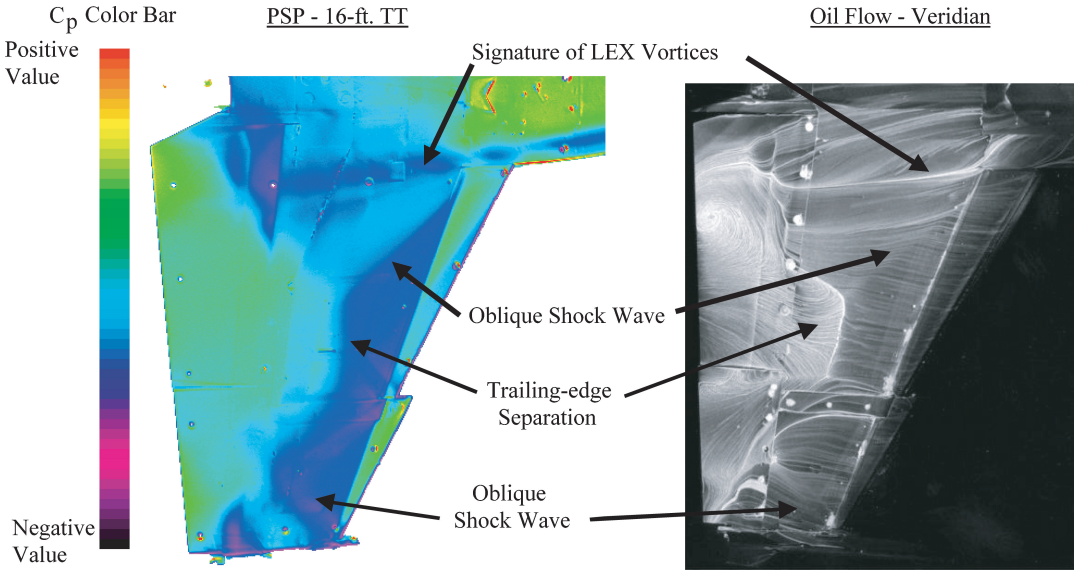

Fig. 8 Comparison of PSP image and oil flow image at $\alpha = 8.0$ deg.

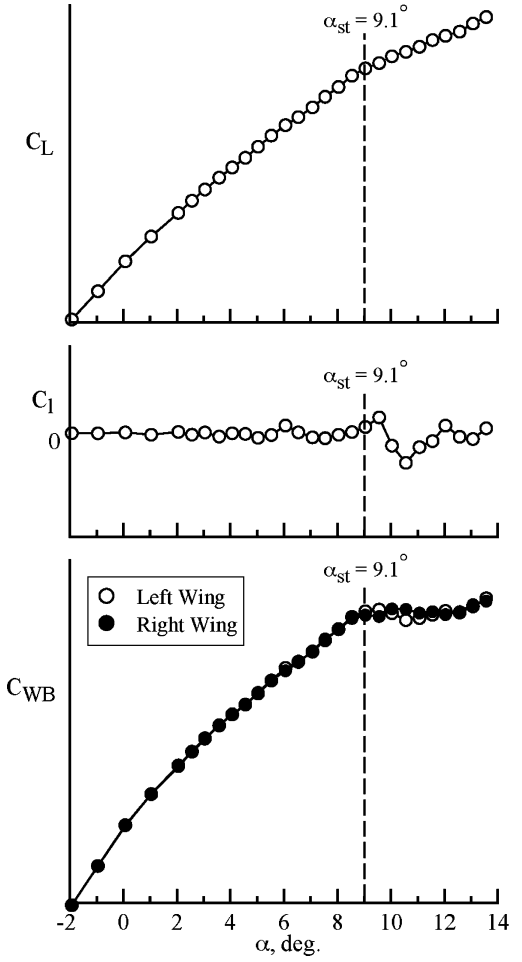

Fig. 9 C_L, C_l, and C_{WM} data for -2 deg $< \alpha <$ 14 deg (run 1334).

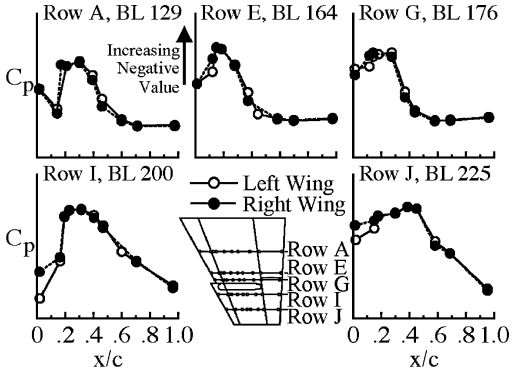

Fig. 10 C_p data at $\alpha = 8.0$ deg (run 1334).

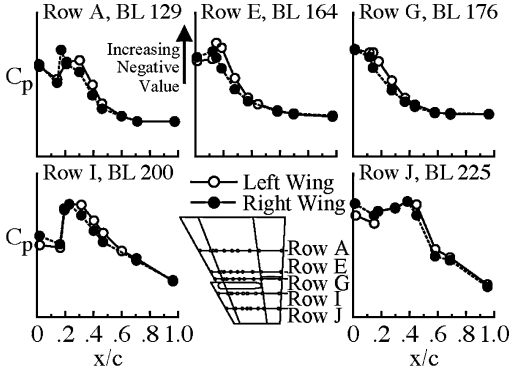

Fig. 11 C_p data at $\alpha = 9.1$ deg (run 1334).

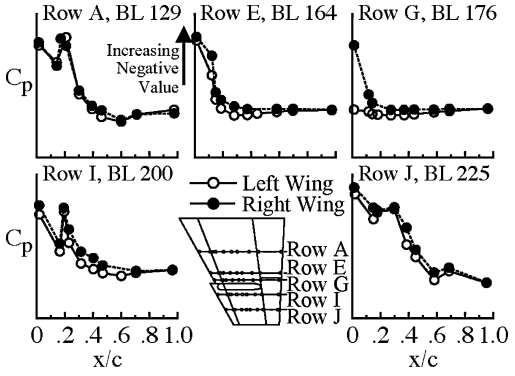

Fig. 12 C_p data at $\alpha = 10.6$ deg (run 1334).

left wing panel at $\alpha = 9.1$ deg. The net result at this angle of attack is a slightly positive value of C_l. However, C_l varies with α, as indicated by the changing sign of C_l. At $\alpha = 10.6$ deg, the left-wing panel has also stalled such that the left-wing panel has less lift and a negative C_l was measured.

The preceding observations are supported by the wing surface coefficient C_p data as shown for representative angles of attack in Figs. 10–12. At $\alpha = 8.0$ deg (Fig. 10), the pressure distributions for all five rows are symmetrical between the left- and right-wing

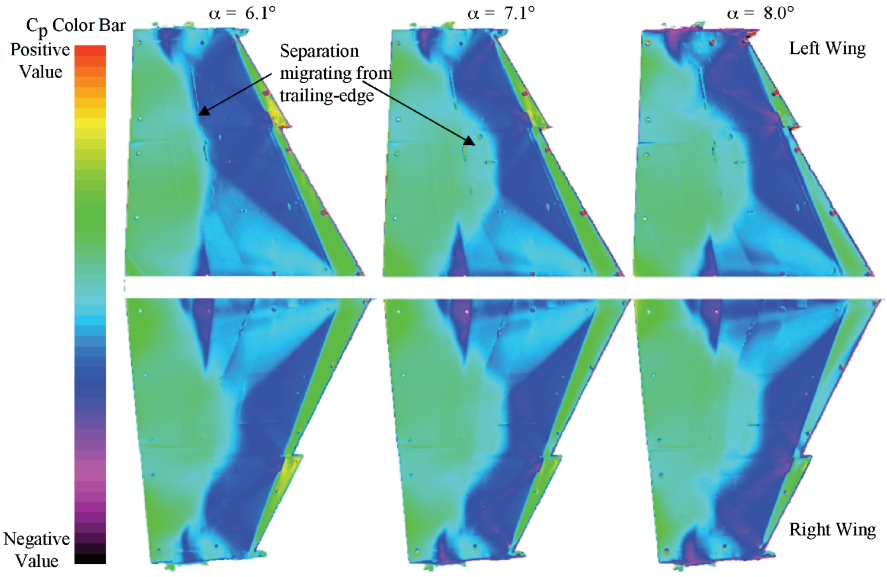

a) $\alpha = 6.1$, 7.1, and 8.0 deg

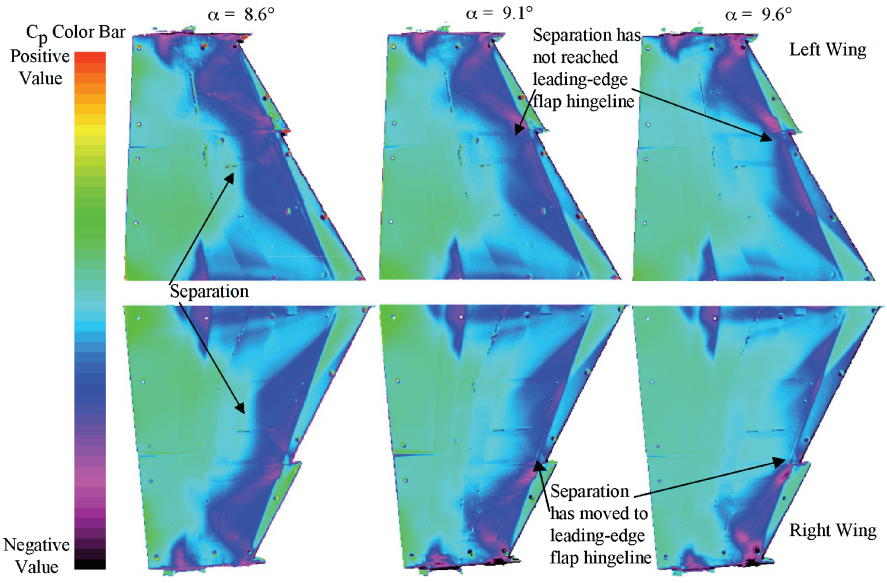

b) $\alpha = 8.6$, 9.1, and 9.6 deg

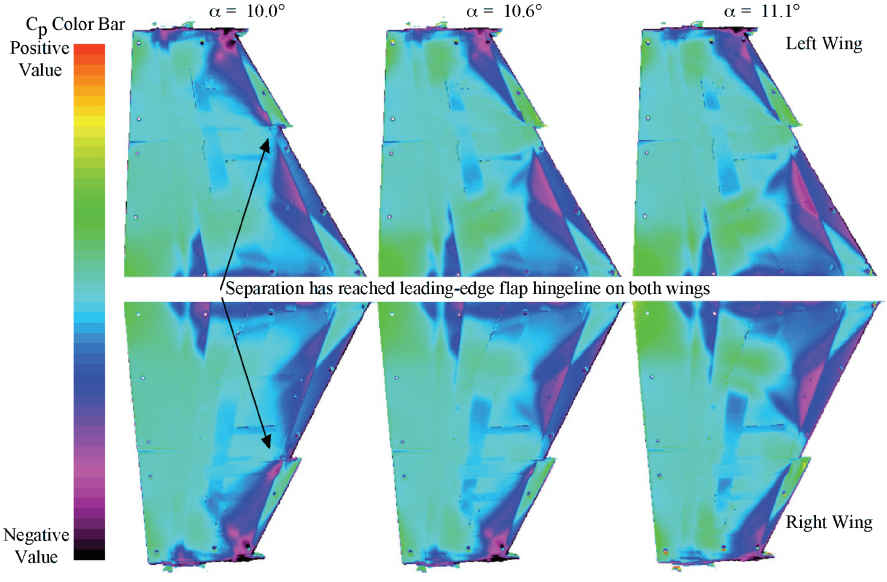

c) $\alpha = 10.0$, 10.6, and 11.1 deg

Fig. 13 PSP data from run 1334 at $M = 0.9$ and various α conditions.

panels. However, at $\alpha = 9.1$ deg (Fig. 11) the right wing has a higher pressure (and thus less suction) near the center of the wing chord and across the span, indicating a loss in lift on the right wing and thus a positive rolling moment. At $\alpha = 10.6$ deg (Fig. 12), the left wing has the higher pressure, indicating a loss in the lift on the left wing (compared to the right wing) and thus a negative rolling moment.

Figure 13 shows PSP data for run 1334 at $\alpha = 6.1$, 7.1, 8.0, 8.6, 9.1, 9.6, 10.0, 10.6, and 11.1 deg. The PSP data of Fig. 13 show several flow features identified in Fig. 8. However, for relevance to the abrupt-wing-stall phenomenon the migration of separation from the trailing-edge to the leading-edge flap is the flow feature to be discussed here. At the lower angles of attack, $\alpha \leq 8.6$ deg, the PSP data clearly show separation at the midspan of the wing advancing from the trailing-edge hingeline towards the leading edge with increasing α. This separation is fairly symmetrical between the right and left wings from 6.1 deg $\leq \alpha \leq 8.6$ deg. At $\alpha = 9.1$ deg, the trailing-edge separation on the right wing suddenly advanced all of the way to the leading-edge flap hingeline just inboard of the leading-edge snag. The separation on the left wing moved forward from its position at $\alpha = 8.6$ deg but did not appear to reach the leading-edge flap hingeline at $\alpha = 9.1$ deg nor at $\alpha = 9.6$ deg. At $\alpha = 10.0$ deg, the PSP data show that the separation reached the leading-edge flap hingeline for both wings.

Recall that the C_{WM} and C_l data of Fig. 9 the C_p data of Fig. 11 showed that, at $\alpha = 10.5$ deg, the left wing had less lift (indicated

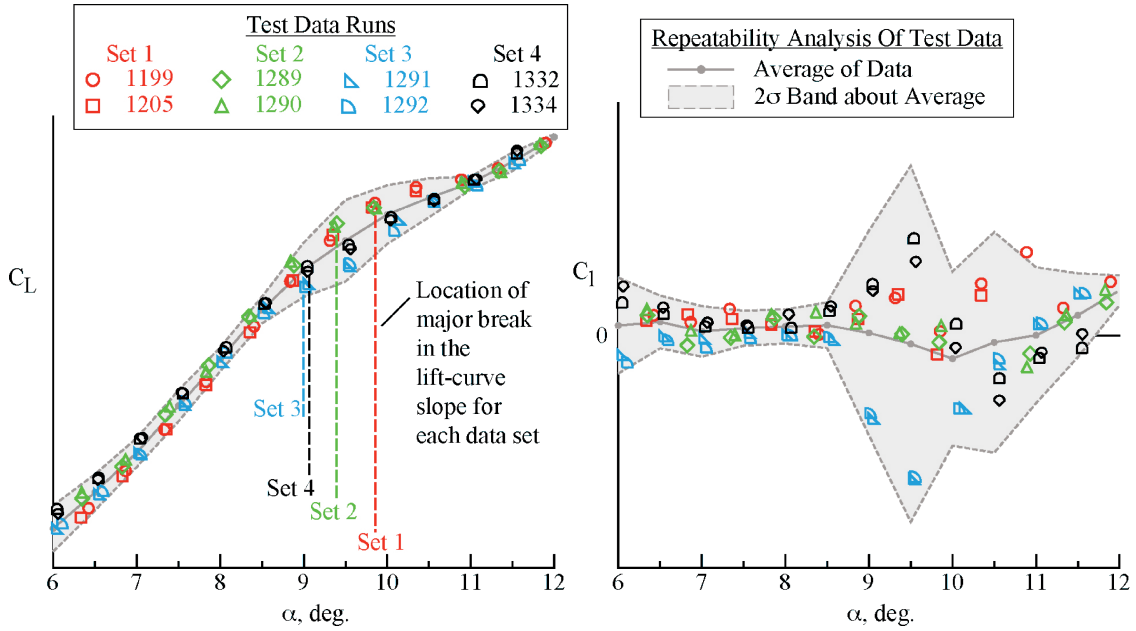

a) C_L and C_l data

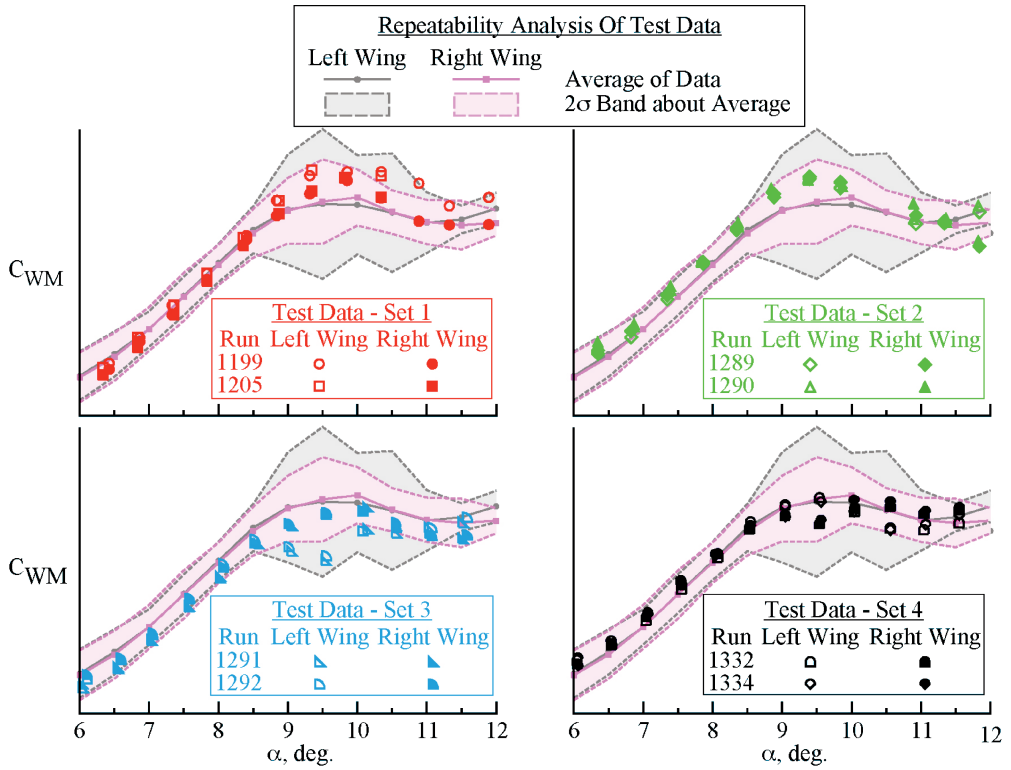

b) C_{WM} data for the left- and right-wing panels

Fig. 14 C_L, C_l, C_{WM}, and repeatability analysis data at $M = 0.9$.

by a lower C_{WM} and greater pressure than was observed on the right wing). The result was a negative rolling moment for the configuration. Although the PSP data do not show any asymmetry in the extent of flow separation features between the left and right wing, the PSP data do show higher values of C_p behind the separation front on the left wing compared to the right wing. This observation corresponds to ESP data of rows I and J on the left and right wings at $\alpha = 10.5$ deg (see Fig. 12). Consequently, there is very good agreement between the PSP images, the ESP pressure data, wing-root bending-moment gauge data, and model balance data.

Repeatability Analysis and Pressure-Sensitive-Paint Data

As discussed in the "Tunnel and Flow Conditions" section, the model would vibrate in a pitch/plunge motion when the model was moved into the critical range near $\alpha = 9$ deg. This vibration can be interpreted as an indicator of the abrupt wing stall occurring on the wing and illustrates the unsteady nature of the stall process.

Another measure of the unsteadiness of the flow phenomena can be found in a repeatability analysis of the data from the test. During the wind-tunnel entry for the PSP data runs, the baseline configuration was tested for a total of eight runs. These runs are grouped into four sets, where a set is defined as a particular installation of flaps and a coating of PSP. These four data sets are referred to hereafter as the baseline data set. Table 1 shows the model changes and PSP changes that occurred between the four sets of data.

Figure 14 shows C_L, C_l, and C_{WM} data for all eight runs. A simple statistical analysis was used to determine the mean (or average) and the standard deviation (σ), at each angle of attack, for the eight runs of data. Figure 14 also shows the averaged data from the baseline data set. The shaded area in Fig. 14 represents the extent of

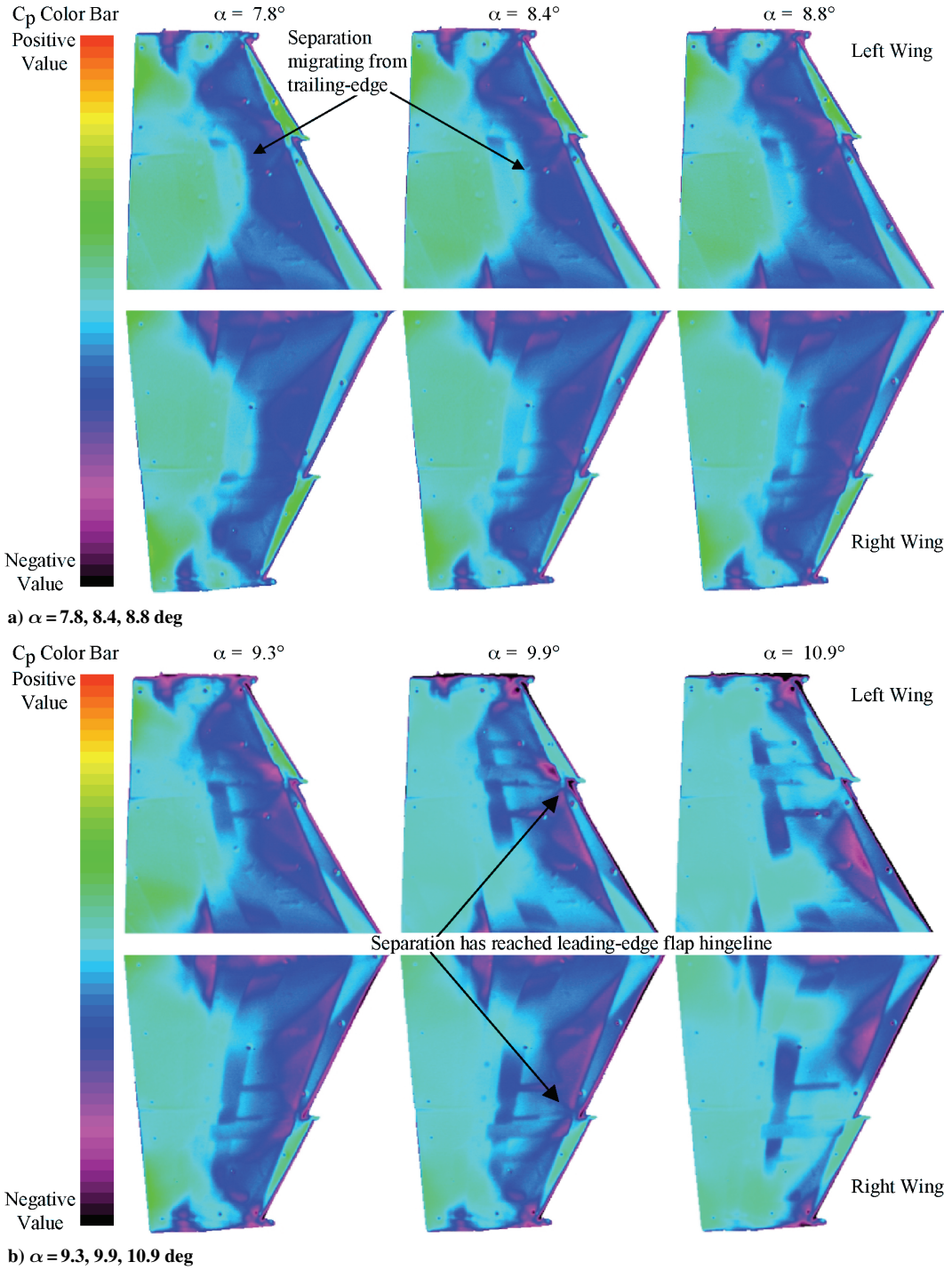

Fig. 15 PSP data from run 1199 at $M = 0.9$ and various α conditions.

Table 1 Model and PSP changes between sets of baseline data

Sets	Model work done
1	First installation of baseline configuration with PSP applied up to trip dots
2	Second installation following 5 configurations and 4 PSP coatings applied
3	Third installation following the removal and reinstallation of sting/balance/model assembly, PSP coating applied
4	Fourth installation following 1 configuration and 1 PSP coating applied

uncertainty in the data, based on a 2σ band around the average of the data. Thus, the 2σ band represents where one would expect 95% of collected data to reside. The standard deviation of the data significantly increases over a 1.5 deg range of α, 9 deg $< \alpha <$ 10.5 deg. As discussed earlier, the model/sting assembly was observed to have a pitch/plunge behavior at this α range, and the intensity of this behavior would vary run to run. In fact, data were not obtained at $\alpha = 10.5$ deg for the set 2 runs because the model dynamics generated unacceptable balance loads preventing a pause at that condition. However, for all of the other runs data were obtained in this α range as the balance loads remained acceptable despite any unsteady pitch/plunge motion of the model/sting assembly. Another reason for the increase in data scatter at 9 deg $< \alpha <$ 10.5 deg is that

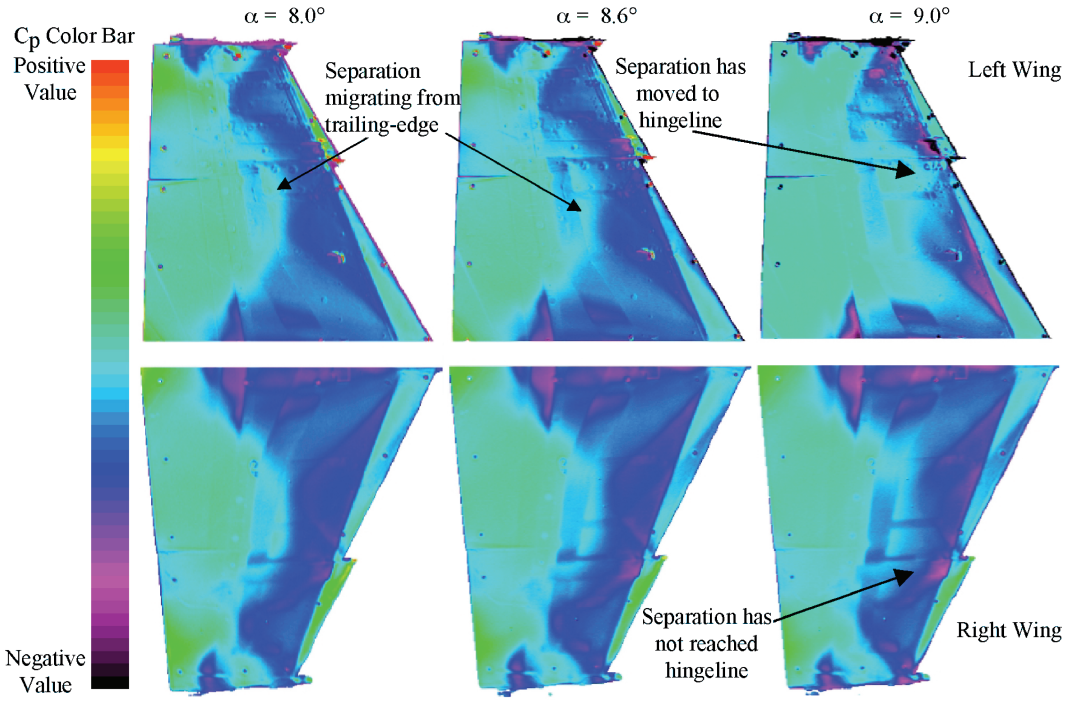

a) $\alpha = 8.0, 8.6, 9.0$ deg

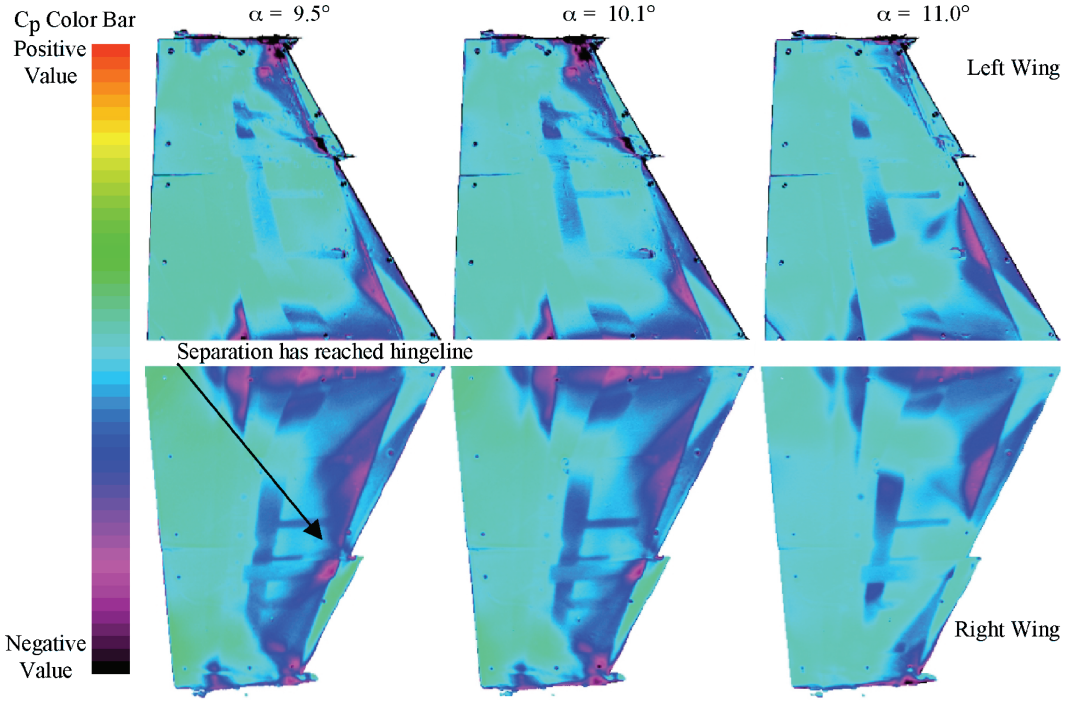

b) $\alpha = 9.5, 10.1, 11.0$ deg

Fig. 16 PSP data from run 1291 at $M = 0.9$ and various α conditions.

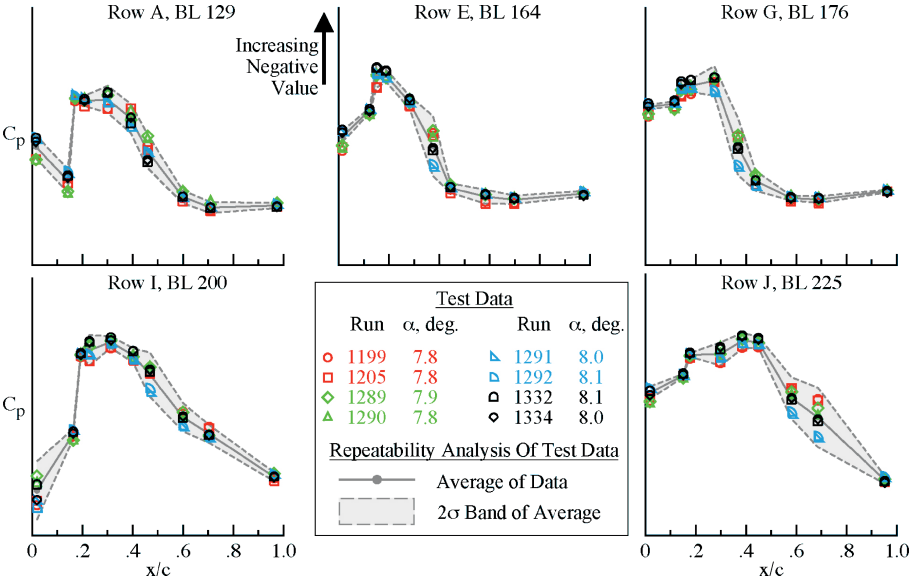

a) $\alpha \sim 8$ deg

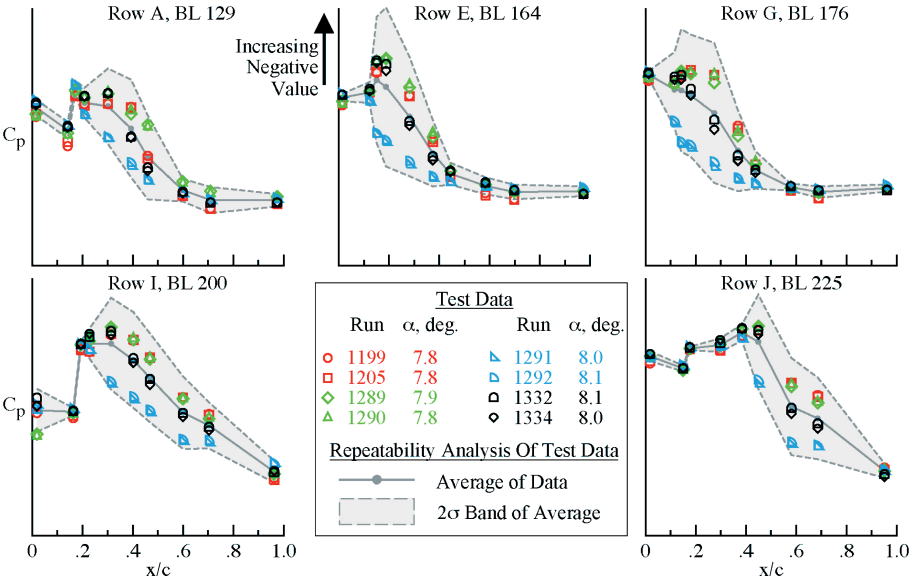

b) $\alpha \sim 9$ deg

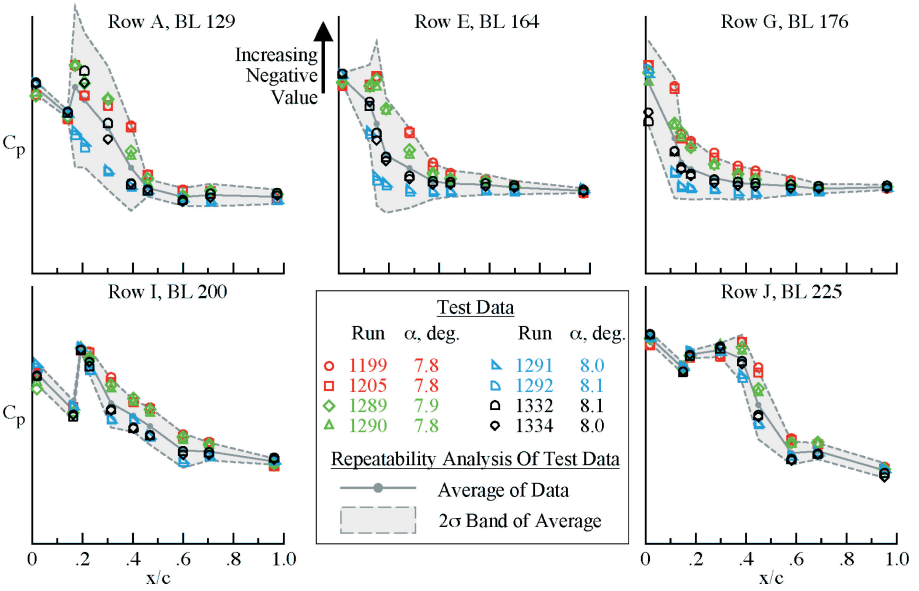

c) $\alpha \sim 10$ deg

Fig. 17 C_P and repeatability analysis data for the eight runs at $M = 0.9$.

each run of the baseline data set experienced wing stall at a slightly different angle of attack as marked in Fig. 14a. Table 2 lists α_{st} for each data set.

Figure 14a and Table 2 show that α_{st} can vary with run and will occur at 9 deg $\leq \alpha \leq$ 9.9 deg. The PSP data also substantiate that wing stall occurred at different angles of attack for different runs. Recall that the PSP data for run 1334 (see Fig. 13) showed that at $\alpha_{st} = 9.1$ deg the separation at the midspan location on the right wing had advanced to the leading-edge flap hingeline. The PSP data for run 1199 from set 1 and run 1334 from set 3 show similar results. Figures 15 and 16 show PSP data for run 1199 and run 1291, respectively, for 8 deg $< \alpha <$ 11 deg. The PSP data of Fig. 15 show the separation for both wing panels as being aft of the leading-edge flap hingeline for $\alpha \leq 9.4$ deg. At $\alpha_{st} = 9.9$ deg, for run 1199, the separation has advanced to the leading-edge flap hingeline. Likewise, for run 1291, the PSP data of Fig. 16 show the separation for both wing panels as being aft of the leading-edge flap hingeline for $\alpha \leq 8.6$ deg. At $\alpha_{st} = 9.0$ deg, for run 1291, the separation on the left-wing panel has advanced to the leading-edge flap hingeline.

Not only did α_{st} vary for different runs, but also the symmetry of the wing stall as recorded in Table 3. The data of Table 3 were obtained by using the PSP data of Figs. 13, 15, and 16 to determine the value of α at which the separation, migrating from the trailing edge at the midspan, reached the leading-edge flap hingeline.

Table 2 Angle of attack of abrupt wing stall for each data set

Data set	α_{st}
1 (runs 1199 and 1205)	9.9
2 (runs 1289 and 1290)	9.4
3 (runs 1291 and 1292)	9.0
4 (runs 1332 and 1334)	9.1

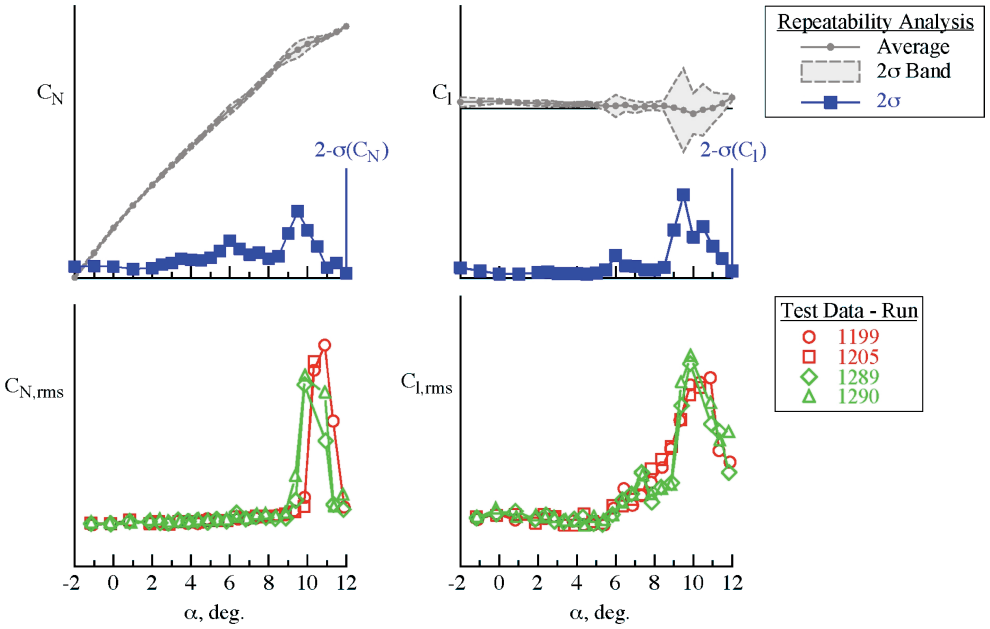

a) C_N and C_l data

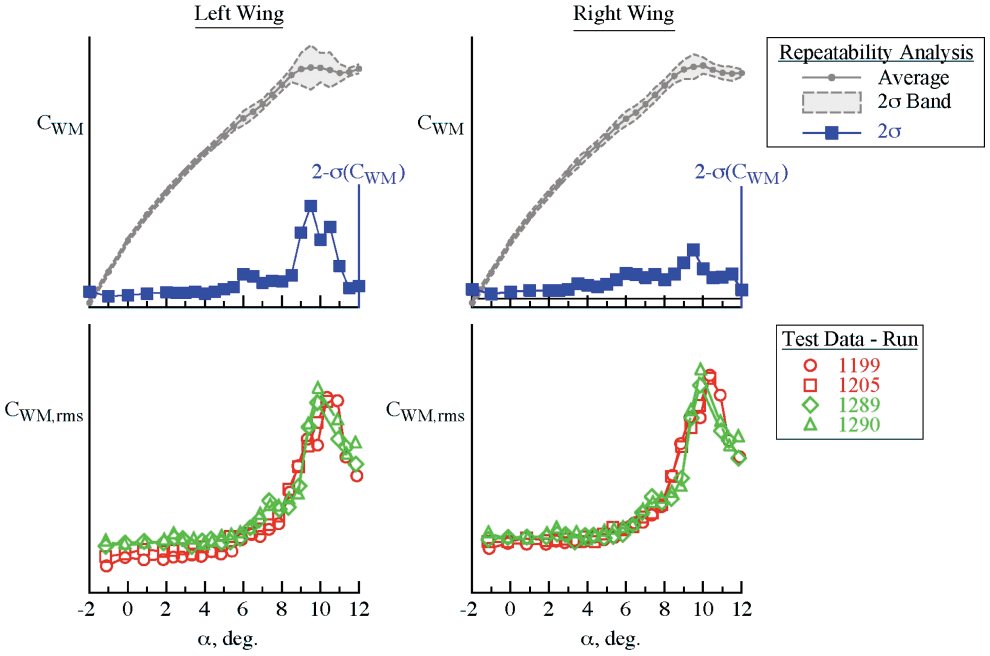

b) C_{WM} data for the left- and right-wing panels

Fig. 18 Comparison of repeatability analysis and measured rms data at $M = 0.9$.

Table 3 Angle of attack where separation has reached the leading-edge flap hingeline

Run	Right-wing panel, deg	Left-wing panel, deg
1199	9.85	9.85
1291	9.52	9.04
1334	9.05	10.05

The symmetry or asymmetry of the wing stall is also evident in the C_l and C_{WM} data of Fig. 14. For run 1334, C_l increases at α_{st} indicating that the right-wing panel has stalled. Note that the data of Fig. 14b show that for run 1334 the break in the C_{WM} vs α curve at $\alpha_{st} = 9.05$ deg is significantly different between the right- and left-wing panels. C_{WM} of the right wing sharply decreases at α_{st}, whereas C_{WM} of the left wing continues a gradual increase in C_{WM} with increase α. The C_{WM} value for the left-wing panel decreases at $\alpha = 10.05$ deg, where the PSP data had shown that the separation on the left-wing panel had reached the leading-edge flap hingeline. The data of run 1291 has similar behavior, although the left-wing panel stalls first. In contrast, the data for sets 1 and 2 do not indicate one wing stalling before the other. For sets 1 and 2, the data do not show a sharp increase or decrease in C_l at α_{st}, nor a sharp slope change in C_{WM} for either wing at α_{st}. Thus, the force/moment data agree with the PSP data in that neither wing panel is dominant in the wing-stall process.

The repeatability analysis was also conducted on the C_p data. Figure 17 shows the data repeatability analysis for the left-wing panel for nominal angles of attack of 8, 9, and 10 deg. At $\alpha \sim 8$ deg, before abrupt wing stall occurs, the pressure data have very little data scatter between the eight runs of data. However, at $\alpha = 9$ deg and $\alpha \sim 10$ deg, the 2σ value (95% confidence level) for the C_p data increases over the wing spar at midspan. This observation corresponds to the fact that the location of the separation in this α range varies for each run as indicated in the PSP data of Figs. 13, 15 and 16. However, at $\alpha = 11$ deg (data not shown here) the 2σ value of the pressure coefficient data has decreased sharply. This observation corresponds to the separation having reached the leading-edge flap hingeline on both wing panels as noted in the PSP data of Figs. 13, 15, and 16.

The repeatability analysis shows a substantial increase in the data scatter (i.e., a loss in the repeatability of the data) in the angle-of-attack range where abrupt wing stall occurs. Abrupt wing stall can occur within a 1 deg α range, is random (neither right or left dominant), and can occur symmetrically or asymmetrically. This random nature of the abrupt wing stall was also observed throughout the F/A-18E/F full-scale aircraft development program for more than one aircraft. However, the angle-of-attack range where abrupt wing stall was observed, that is, $9 < \alpha < 10$ deg, is about 1 deg higher than that observed in the F/A-18E/F full-scale aircraft development program. The flap setting of 10 deg/10 deg/5 deg at $M = 0.9$ and $\alpha = 9$ deg is not on the flap schedule for the full-scale aircraft.

RMS Measurements

The fact that the same flap-set configuration installed at different times within a wind-tunnel test entry can stall at slightly different angles is indicative of the sensitive and dynamic nature of abrupt wing stall. Another approach to capturing the level of unsteadiness occurring over the wing panels was to use rms instrumentation that calculated running values of rms for the respective signals. This value of rms was then recorded as a time-averaged measurement in the same manner as the static data. Figure 18 show the time-averaged measurement of rms, denoted by the subscript rms, for the normal force, rolling moment, and the two wing-root bending-moment gauges for runs from sets 1 and 2. The rms instrumentation was not in use when runs in sets 3 and 4 were conducted.

Figure 18 also shows the statistical data generated from the baseline data set. Note that the normal force data are plotted instead of C_L because only the balance component signals were recorded thorough the rms boards. The repeatability analysis data are presented in two forms in upper plots of Fig. 18. The first form is the plot of the averaged data with a shaded area representing the 2σ of the data set. The second form is a line plot of the 2σ variable shown on the right axis. The scale for the right axis has been scaled up to show features of the 2σ value with respect to angle of attack.

Figure 18 shows the data over -2 deg $< \alpha < 12$ deg. Note that at the lower angles of attack, $\alpha < 6$ deg, both the time-averaged measured rms and 2σ variable are fairly constant with increasing angle of attack. This trend would indicate that the model is not experiencing unsteady forces/moments. Indeed, for $\alpha < 9$ deg the model was not observed to be vibrating on the sting. At $\alpha = 6$ deg, the time-averaged measured rms and 2σ variables show slight increases, which then decrease at $\alpha = 7$ deg. This spike in the rms corresponds to the trailing-edge separation at the midspan of the wing advancing from the trailing-edge flap onto the wing spar as seen in the PSP data of Fig. 13a.

Recall from the "Static and PSP Data" section that the model would vibrate under dynamic loads for the angle-of attack-range of 9 to 10 deg. The data show a marked increase in the rms of each coefficient at this angle-of-attack range. This sharp increase in rms corresponds to an increase in the 2σ value from repeatability analysis conducted on the baseline data set. Because an increase in rms denotes an increase in unsteadiness of that signal from the balance or strain gauge, the increase in 2σ (which denotes an increase in data scatter between the eight data runs) can also be interpreted to indicate an increase in unsteadiness in the flow over the wings.

Time History Measurements

Another approach to capturing the level of unsteadiness of the flow over the wing panels was to record the time histories of the instrument signals. Thus, a complete dynamic analysis could be conducted as was done on the baseline configuration in Ref. 4. This discussion will compare the repeatability analysis, static data and rms measurements to the average and rms of the time history for several parameters. Figure 19 combines the C_l data from the three separate sets of data on the baseline configuration. The three sets of data are as follows: 1) repeatability analysis data, 2) static data, and 3) time history data. The first data set uses the repeatability analysis conducted for the baseline data set from the PSP test runs. The average and 2σ values, calculated from the eight runs of data, are shown here. The static data and time history data are from one run of data (run 20) for which static data and the time histories of several instruments were recorded. The second data set uses the static (or

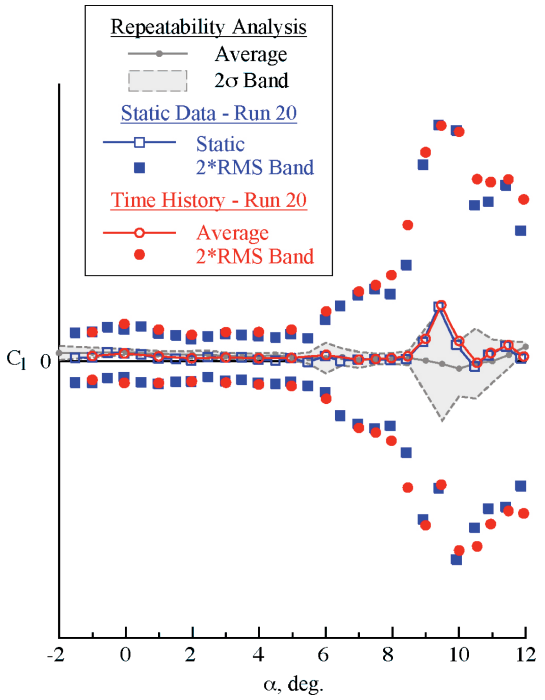

Fig. 19 Comparison of repeatability analysis, static data, and time history data at $M = 0.9$.

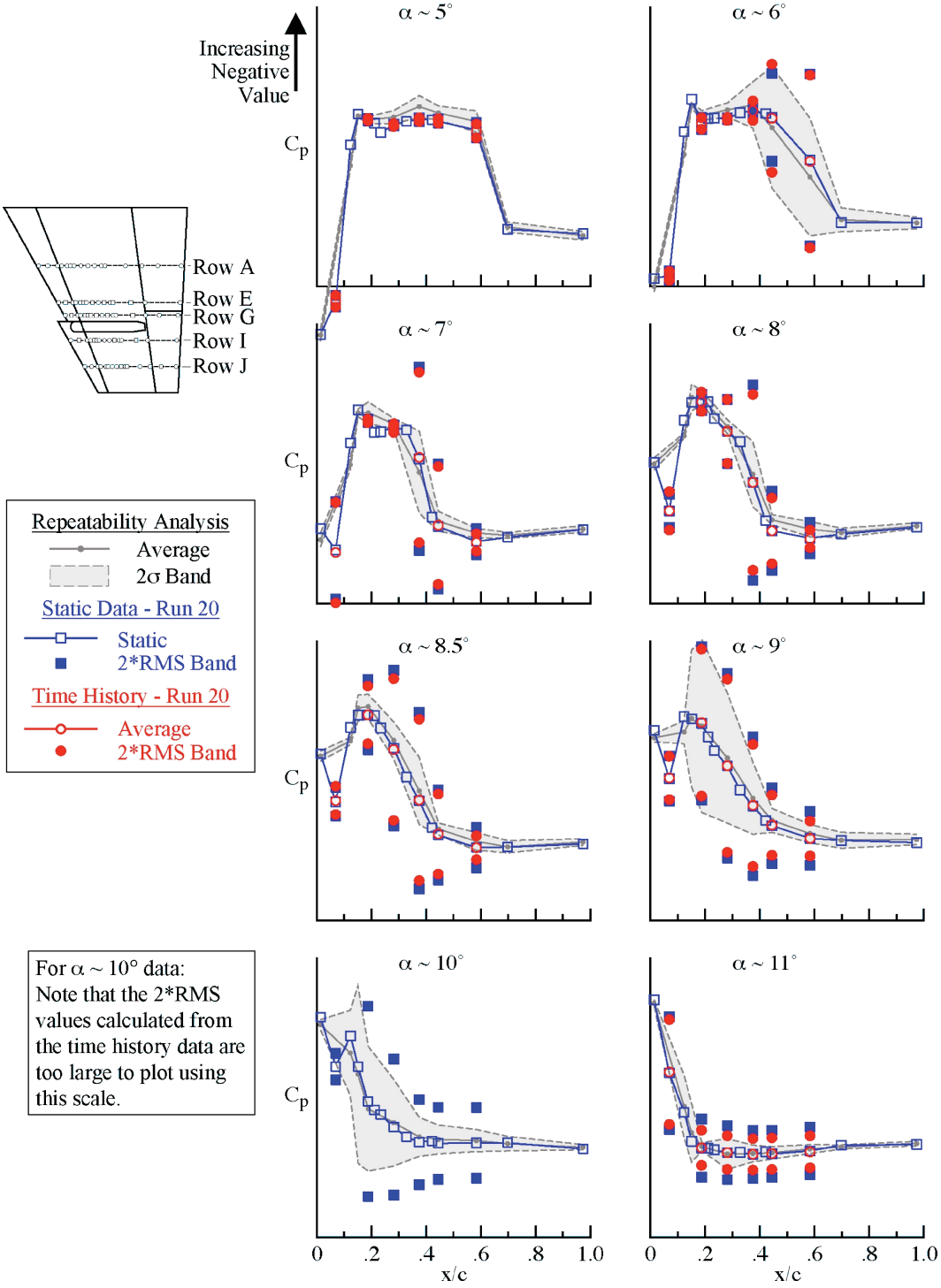

Fig. 20 C_p **data from the repeatability analysis, static, and time history data sets at** $M = 0.9$ **and various angles of attack for row E.**

time-averaged) value of C_l. The rms of the rolling-moment balance component as measured through the rms board is also shown as part of the static data set. For the third data set, an average of C_l was derived from the time history data. This average was subtracted from each data point of the time history data, and the resulting values were used to calculate standard deviation, or rms, for the time history data.

The average C_l derived from the time history of run 20 agrees well with the static (time-averaged) value of C_l. Note that both values of C_l fall within the 2σ band of the repeatability analysis. Also note that the rms derived from the time history and the rms measured as a time-averaged parameter agree very well in terms of magnitude and trend with angle of attack. However, the most striking observation is the trend of the rms from the time history with respect to angle of attack. Although the magnitude of the 2*rms parameter is considerably more than that of the 2σ value, both parameters significantly increase over a very small angle-of-attack range (8.5 deg $< \alpha <$ 9 deg) and maintain an elevated level for about an α increment of 1.5 deg (9 deg $< \alpha <$ 10.5 deg) before returning to a lower value.

A similar comparison was made for the surface-pressure coefficient data with mixed results. Figure 20 shows the C_p data from the three data sets just defined at several angles of attack. The time history data set consists of the 15 unsteady pressure transducers on the left wing. The 15 unsteady pressure transducers were the only pressure transducers routed through the rms boards so that the time-averaged data set only has rms data for 15 of the pressure ports. The $\alpha \sim 5$ deg data of Fig. 20 show that the average C_p data, derived from

the time history data of the unsteady pressure transducers, agree well with the static C_p data. The standard deviation data from all three data sets are small and indicate very little unsteady effects. At $\alpha \sim 6$ deg, the C_p derived from the time history agrees well with the static C_p data. Also, the 2*rms values from both the time-averaged and time history data sets indicate a sharp increase in unsteadiness. This result corresponds to an increase in the 2σ value derived from the repeatability analysis. As just discussed, this activity is probably caused by the separation moving from the trailing-edge flap onto the wing spar as seen in the PSP data of Fig. 13a.

The repeatability analysis data show that once the angle of attack was increased to 7 deg, the 2σ value decreased sharply to a similar value as that observed before $\alpha \sim 6$ deg. In contrast, the 2*rms data show that not all of the unsteady transducers returned to a low dynamic activity. Rather, those transducers near midchord and midspan still experienced some dynamic activity, which is expected to be the result of mild shock oscillations that are identified in Ref. 4. This trend remained until $\alpha \sim 8.5$ deg, when the 2*rms values for all of the transducers at midspan increased and continued to increase with angle of attack. In fact at $\alpha \sim 10$ deg, the C_p and 2*rms values from the time history data do not agree with the static data. In fact, these values are so greater than the plot maximums and thus do not appear in the plots. The 2σ value from the repeatability analysis do not experience a significant increase until $\alpha \sim 9$ deg and are smaller in comparison to the time history data. The time history measurements are clearly more sensitive to the approach of abrupt wing stall than the repeatability analysis, which is to be expected because all of the data in the baseline data set have been passed through a low-pass frequency filter before being measured by the data system. Note that at $\alpha \sim 11$ deg after the midwing has stalled, both the 2σ and 2*rms data return to low values seen before the dynamic activity was encountered at $\alpha \sim 6$ deg.

Lessons Learned

The technical approach taken to observe and analyze the unsteady abrupt wing stall occurring on the 8% F/A-18E/F model has yielded not only information on the wing-stall process, but also on the experimental techniques used. The lessons learned are listed here:

1) The angle-of-attack increment required to capture the abrupt stall process was 0.5 deg. A test conducted using conventional increments of α (1 or greater) would have missed the critical features of the phenomenon.

2) Trenches for pressure tubing and wiring should be limited to the lower surface of wings to minimize the impact of the fill material in the trenches during PSP testing.

3) For the paint used in this study, the model had to be at room temperature before the PSP coat can be applied. The need for the model to cool down after running greatly increased down time in the wind tunnel between configuration changes.

4) The need to obtain wind-off data after 1, or at most 2, runs greatly increased the length of time needed to test one configuration.

5) Care and sensitivity to potential impacts on data are needed during the application of trip dots and other model features that might affect the aerodynamic performance of the leading-edge flaps.

6) Repeat runs should be included in a test program and can be used to clarify unsteady or repeatability issues.

Summary

A wind-tunnel test of a preproduction 8% F/A-18E model at $M = 0.90$ was conducted in the NASA Langley Research Center 16-ft TT to investigate on-surface flow physics during wing stall. The technical approach employed focused on correlating static (or time-averaged) and unsteady wind-tunnel test data to the unsteady wing-stall events using force, moment, pressure, and pressure-sensitive-paint measurements. The abrupt wing stall experienced by the 8% F/A-18E model was observed to be an unsteady event occurring when the separation, which had migrated forward from the trailing edge, rapidly advanced to the leading-edge flap hingeline for a very small increment in angle of attack. The angle of attack at which wing stall occurred varied, from run to run, over a 1-deg increment. The abrupt wing stall can occur simultaneously on both wing panels or asymmetrically. Asymmetric rolling moment occurs if the wing stall occurs asymmetrically. As angle of attack is further increased, both wing panels stall and the large roll asymmetries are significantly reduced.

Several techniques were used to capture abrupt wing stall in a conventional wind-tunnel setup. The pressure-sensitive-paint technique provided global looks at the flow structures occurring over the wing before and during wing stall. Pressure-sensitive-paint data and wing-root bending-moment strain gauges data provided insight to the asymmetry (or symmetry) of the abrupt-wing-stall process. A simple repeatability analysis was conducted on the static data from eight runs on the preproduction F/A-18E configuration. The standard deviation σ value was observed to be an indicator of unsteadiness in the flow over the wing. The repeatability analysis provided a quick and inexpensive examination of the unsteady aerodynamic characteristics of abrupt wing stall and was surprisingly accurate when compared to unsteady measurements of pressures and rolling moment. This approach could be used to identify test conditions at which a more complex and detailed examination of unsteady data could be conducted.

References

[1]Hall, R., and Woodson, S., "Introduction to the Abrupt Wing Stall (AWS) Program," *Journal of Aircraft*, Vol. 41, No. 3, 2004, pp. 425–435.

[2]Capone, F. J., Bangert, L. S., Asbury, S. C., Mills, C. T. L., and Bare, E. A., "The NASA Langley 16 Foot Transonic Tunnel—Historical Overview, Facility Description, Calibration, Flow Characteristics, and Test Capabilities," NASA TP 3521, Oct. 1995.

[3]Schuster, David M., and Byrd, James E., "Transonic Unsteady Aerodynamics of the F/A-18E at Conditions Promoting Abrupt Wing Stall," *Journal of Aircraft*, Vol. 41, No. 3, 2004, pp. 485–492.

[4]Sprinkle, D. R., Obara, C. J., Amer, T. R., Leighty, B. D., Carmine, M. T., Burkett, C. G., and Sealey, B. S., "Langley 16-Ft. Transonic Tunnel Pressure Sensitive Paint System," NASA TM-2001-211017, June 2001.